Moho map of South America from receiver functions and surface waves

Simon Lloyd,[1] Suzan van der Lee,[1] George Sand França,[2] Marcelo Assumpção,[3] and Mei Feng[4]

[1]   We estimate crustal structure and thickness of South America north of roughly 40°S. To this end, we analyzed receiver functions from 20 relatively new temporary broadband seismic stations deployed across eastern Brazil. In the analysis we include teleseismic and some regional events, particularly for stations that recorded few suitable earthquakes. We first estimate crustal thickness and average Poisson's ratio using two different stacking methods. We then combine the new crustal constraints with results from previous receiver function studies. To interpolate the crustal thickness between the station locations, we jointly invert these Moho point constraints, Rayleigh wave group velocities, and regional S and Rayleigh waveforms for a continuous map of Moho depth. The new tomographic Moho map suggests that Moho depth and Moho relief vary slightly with age within the Precambrian crust. Whether or not a positive correlation between crustal thickness and geologic age is derived from the pre-interpolation point constraints depends strongly on the selected subset of receiver functions. This implies that using only pre-interpolation point constraints (receiver functions) inadequately samples the spatial variation in geologic age. The new Moho map also reveals an anomalously deep Moho beneath the oldest core of the Amazonian Craton.

1.   Introduction

[2]   The South American continent consists of three major roughly N–S oriented geologic domains [*Beurlen*, 1970]. These are the Pacific margin with the Andes, the wide lowland areas east of the Andes running from the Argentinian Pampa to eastern Columbia, and the Precambrian portion of South America to the east. These three domains are easily identified topographically; the Andes include impressive mountain ranges and volcanoes, which have been active since the beginning of the Mesozoic, the interior lowlands are relatively flat, while the relief of Precambrian eastern South America is surprisingly uneven (Figure 1). The later includes the Amazonian craton, which contains the Guyana and Guaporé shields and the Amazonas basin which separates the two shields. The tectonic processes responsible for the current landscape were most active during the Lower Cretaceous.

These processes continued through the Tertiary [*de Almeida et al.*, 2000; *Beurlen*, 1970] and there are indications for current tectonic activity [*Riccomini and Assumpção*, 1999].

[3]   The tectonic forces responsible for the observed differences likely also left an imprint beneath the surface. Understanding these subsurface structures may therefore help unravel the evolution of the South American continent. We use seismology to investigate the Earth's interior, and provide additional information about the evolution and current state of the crust and upper mantle beneath South America. Within the past decade the availability of seismological data recorded in South America has improved drastically. However, the majority has been in the form of temporary deployments on the active Pacific margin [e.g., *Beck et al.*, 1996; *Yuan et al.*, 2002]. The lack of continent-wide station coverage has prevented extensive geophysical studies of Precambrian South America. So far, seismic studies have been restricted to global studies or smaller subregions [e.g., *Assumpção et al.*, 2002, 2004]. With the Brazilian Lithosphere Seismic Project 2002 (BLSP02) [*Feng et al.*, 2004], the situation improved, as 20 temporary broadband seismic stations were deployed throughout eastern Brazil (Figure 1). They recorded earthquakes within the period of 2001 to 2004, of which many have their origin in the subduction zone on the western South American margin. In this paper we analyze receiver functions of these data, and provide geophysical constraints on crustal thickness and structure beneath the station locations. We

[1]Department of Earth and Planetary Sciences, Northwestern University, Evanston, Illinois, USA.
[2]Observatório Sismológico-I1G/UnB, Campus Universitário Darci Ribeiro, Brasilia, Brazil.
[3]Institute of Astronomy and Geophysics, University of São Paulo, São Paulo, Brazil.
[4]Institute of Geomechanics, Chinese Academy of Geological Sciences, Beijing, China.
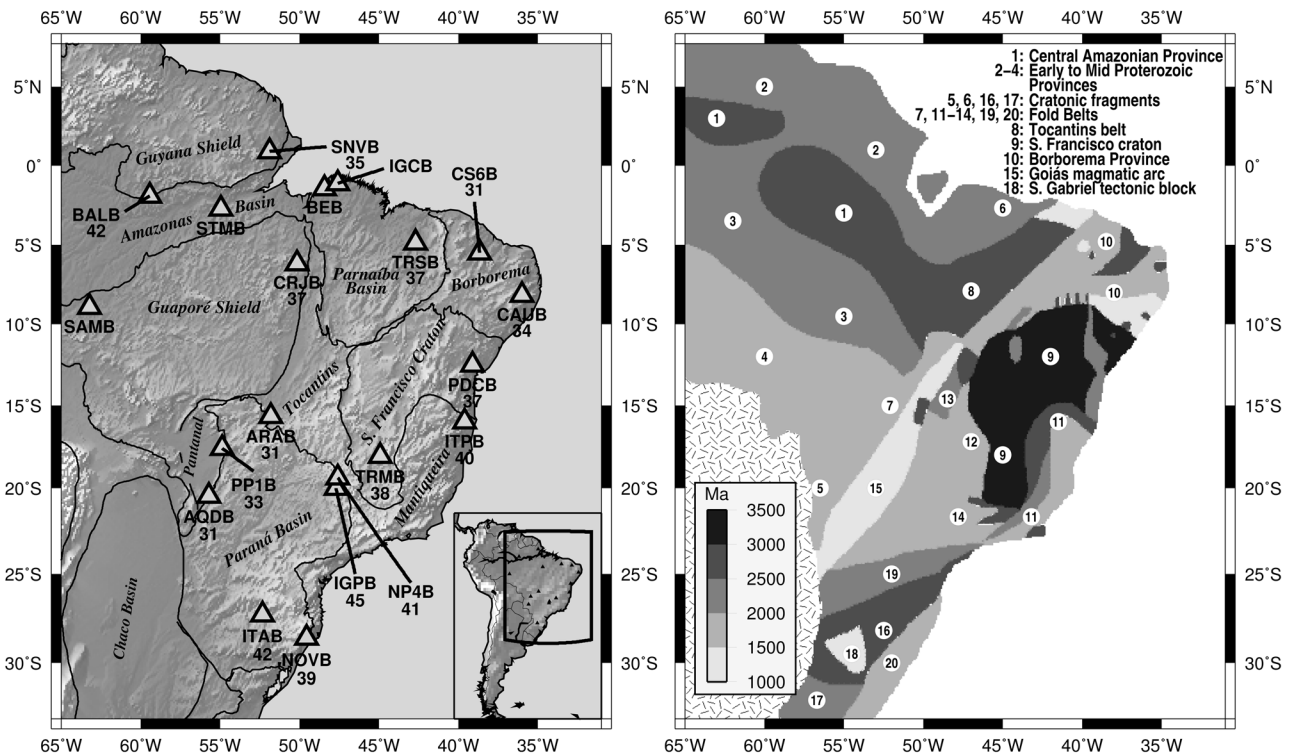
Figure 1. (left) Tectonic provinces of Precambrian South America and the locations of the 20 BLSP02 temporary broadband seismic stations (STS2) providing the earthquake data for RF analysis in this study. The numbers beneath the station names are the crustal thickness in km we determined in this study. (right) Crustal ages used in this study [after *Cordani and Sato*, 1999].

combine our results with receiver function (RF) constraints from the literature to investigate a possible correlation between crustal structure and crustal age [*Durrheim and Mooney*, 1991, 1994; *Zandt and Ammon*, 1995]. To estimate crustal thickness between station locations, we jointly invert these point constraints from RF analysis with Rayleigh wave group velocities and regional *S* and Rayleigh waveforms. The result of this joint inversion is a continuous map of Moho depth for most of South America. Using this map to investigate a possible correlation between age and structure of the crust reduces possible bias from the spatially restricted and nonuniform sampling of RFs alone.

1.1. Precambrian South America

[4] Understanding the past and active processes defining the current state of Precambrian cratons worldwide is key for unraveling Earth's early history. However, Precambrian South America has not been studied as extensively as other continents. This is shown by the small amount of South American data used in global compilations studying the crust [e.g., *Christensen and Mooney*, 1995].

[5] Precambrian South American is predominantly Proterozoic in age [*Cordani and Sato*, 1999], and has undergone several phases of continental collision and subsequent breakup. The resulting current state is a composite of Archean and Proterozoic cratonic areas separated by collisional belts [e.g., *de Almeida et al.*, 2000]. The Archean nuclei have undergone significant structural reworking, magmatism and heating mostly during the first (the Trans-Amazonian, 2.2–

1.8 Ga) of three major Proterozoic orogens [*de Almeida et al.*, 2000]. Multiple basinal regions such as the Amazonian rift subdividing the Amazonian craton [*Tassinari and Macambira*, 1999], and the Paraná flood basalt province are expressions of an extensional regime occurring after the Neoproterozoic Brasiliano collage [*de Almeida et al.*, 2000]. Reactivation of rifts may have played an important role during the Africa–South America breakup in the Mesozoic [*Jacques*, 2003]. During this time period, flood basalts filled most of the Paraná basin, resulting in one of the world's major Large Igneous Provinces (LIP) [*Coffin and Eldholm*, 1994]. The magmatic processes extended into the Argentinian Chaco basin. They were very fast, lasting only 10 Ma between 137 and 127 Ma [*Turner et al.*, 1994], and have been interpreted as surface expressions of the Tristan da Cunha plume.

2. Method

2.1. Receiver Functions

[6] RF analysis makes use of converted *P* to *S* phases at discontinuities in the Earth's interior and has become a standard method to determine crustal thickness or other discontinuous changes in physical properties in the Lithosphere [e.g., *Langston*, 1979; *Owens et al.*, 1984; *Ammon et al.*, 1990; *Kind et al.*, 1995]. Typically, events used for RF analysis have an epicentral distance of $30° \leq \Delta \leq 90°$. The 30° minimum distance prevents the *P* to *S* conversion point from being too far away laterally from the station, and the 90° maximum distance requirement prevents using events
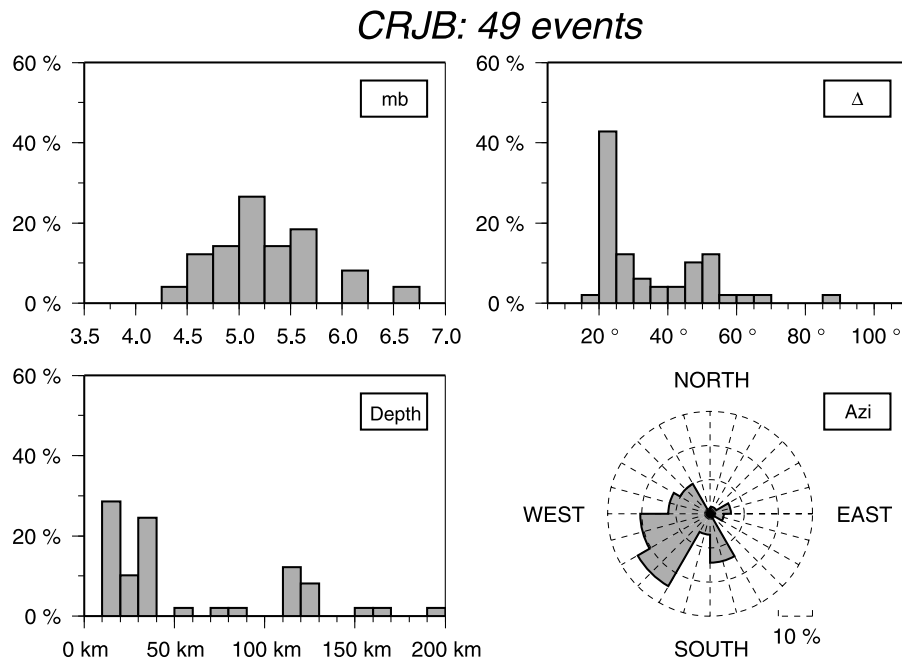
Figure 2. Distribution of the events used for station CRJB.

with only small amplitudes in the converted phases. However, these boundaries are somewhat arbitrary, and since relatively few data are available for some of the stations used for this study, we include events which are closer than 30°. Similarly, we do not impose any restrictions on earthquake magnitude to select events for RF analysis (Figure 2).

[7] We use a water level deconvolution method [*Ammon*, 1991] (deconvolution and RF inversion codes used: http://eqseis.geosc.psu.edu/~cammon/HTML/RftnDocs/rftn01.html) to compute receiver functions, setting filter and deconvolution parameters for each station individually. To determine the crustal thickness H and Poisson's ratio ν beneath each station we proceed by using two grid search methods. The first is the $H - \kappa$ stacking method developed by *Zhu and Kanamori* [2000] (since $\kappa = V_P/V_S$ and $\nu = (V_S^2 - 0.5V_P^2)/(V_S^2 - V_P^2)$, κ is directly related to ν; an increased ν results in an increased κ and vice versa). It uses the RF amplitudes at predicted arrival times of the Moho converted phase (*Ps*) and reverberations (*PpPs* and *PpSs + PsPs*). Taking the slowness p into account (move out depends on p), these times are calculated for a given Moho depth H and Poisson's ratio ν, at which the RF amplitudes are stacked. This is done over a (H, ν) grid, in which the location of the maximum in the grid is the preferred crustal thickness and Poisson's ratio estimate for this station. The inclusion of reverberations in this as well as the following method significantly reduces the trade off that exists in RF inversions between Moho depth and crustal velocities. This is so because the functions describing the trade off are different for the direct *Ps* and reverberated arrivals. Therefore, using both direct and reverberated arrivals in the grid search leads to a well-constrained Moho depth estimate.

[8] The second method we use is the waveform misfit stacking by *Van der Meijde et al.* [2003]. It is similar to the *H - κ* method, but involves computing waveform misfits between synthetic and observed RFs over a (H, ν) grid instead of single amplitudes at particular times. The synthetics are calculated with the program *respknt*, which is based on the method described by *Kennett* [1983].

[9] The time window used to calculate the misfit starts 2 s before and ends 30 s after the direct *P* arrival. Therefore, the direct *P* arrival also contributes to the misfit, which is important when sedimentary layers produce wave conversions and reverberations as well. Again, we perform a grid search to find Crustal thickness and Poisson's ratio. Here the location of the minimum in the grid is the preferred crustal thickness and Poisson's ratio estimate for each station.

[10] For both stacking methods the error estimate is derived from the standard deviation of the mean at the preferred (H, ν) location of the stacked misfits or amplitudes, respectively. We then place a contour in our grid at this level defining the uncertainty in H and ν. Therefore, the sharpness of the peak has an influence on the estimated uncertainty; the sharper it is, the smaller the error becomes. We average the crustal thickness and Poisson's ratios obtained from both methods for each station and combine our results with results of previous studies to investigate possible trends in crustal thickness with age or tectonic domain [*Krüger et al.*, 2002; *Assumpção et al.*, 2002, 2003, 2004; *França and Assumpção*, 2004; *An and Assumpção*, 2006].

[11] In a final step we use our newly obtained crustal thickness estimates as constraints for RF inversion for intracrustal features. We invert stacked RFs for seismic velocities and density of a crustal model consisting of 3–4 layers using the codes of *Ammon* [1991]. We use trial and error style adjustment of the layer depths in the starting model, which provides greater control over the inversion compared to using many thin layers in a smoother model to automatically obtain a satisfactory waveform fit. During the inversion, layer depths (including the depth to the Moho) are held constant. Optimal depths for the layer boundaries are obtained interactively by a

trial and error procedure. Allowing crustal thickness to vary may also improve the waveform fit. However, since the crustal thickness obtained from the grid search is more robust, an optimum waveform fit thanks to crustal thickness adjustment may not necessarily mean the best solution was obtained. Because move out corrections for discontinuities as shallow as the Moho only minimally affect the stack, we stack the observed RFs without move out correction and use their mean slowness to compute the synthetic RF during the inversion.

2.2. Moho Map

[12] We obtain a new Moho map from jointly inverting group velocity measurements of roughly 6600 wave paths [*Feng et al.*, 2004], 1700 waveforms [*Feng et al.*, 2007; *van der Lee et al.*, 2001], and 225 Moho depth point constraints (new ones from this study together with the continent-wide compilation by *Feng et al.* [2004]), of which 67 lie in Precambrian provinces. For the oceanic parts of our model, where no point constraints are available, we insert predicted values from Crust2.0 [*Bassin et al.*, 2000] in order to minimize the trade-off between Moho depth and mantle structure beneath the oceans. Figure 3 shows the wave path coverage for the group velocities and waveform constraints as well as the Moho depth point constraints. The group velocity wave paths cover most of continental South America in a dense pattern (Figure 3, left). Only the most southern parts of Chile and Argentina are not covered. The paths of the waveforms used for the inversion are shown in Figure 3 (right). They are not as dense as the group velocity paths because they rely on the availability of accurate source mechanisms, but they extend beyond continental South America into the Pacific and Atlantic oceans. For each wave path, noncorrelated functions describing a path averaged 1D model are derived using the first step (nonlinear inversion) of the partitioned waveform inversion PWI [*van der Lee and Nolet*, 1997]. For the joint inversion we weight all the data by their respective inverse estimated uncertainty. In addition, we assign weights λ to the three different data sets **q** and corresponding sensitivity kernels **H** to make sure their respective variance reductions are significant and reasonable. That way we prevent any single data set dominating the final Moho model [e.g., *Feng et al.*, 2007; *Chang et al.*, 2010]. Adding regularization (damping) our problem looks as follows:

$$\begin{pmatrix} \lambda_{WF}\mathbf{H_{WF}} \\ \lambda_{VG}\mathbf{H_{VG}} \\ \lambda_{RF}\mathbf{H_{RF}} \\ \lambda_r\mathbf{I} \end{pmatrix} \mathbf{m} = \begin{pmatrix} \lambda_{WF}\mathbf{q_{WF}} \\ \lambda_{VG}\mathbf{q_{VG}} \\ \lambda_{RF}\mathbf{q_{RF}} \\ 0 \end{pmatrix}, \qquad (1)$$

whereby subscripts WF, VG, and RF correspond to waveforms, group velocities, and receiver functions, respectively. The model parameters **m** are obtained solving this system with the LSQR algorithm [*Paige and Saunders*, 1982].

3. Results

3.1. Crustal Thickness and Poisson's Ratio

[13] The crustal thickness and Poisson's ratios obtained with both RF stacking methods are summarized in Table 1. Figures 4 and 5 show examples of contour plots over the

(H - ν) grid of station CRJB for the waveform stacking [*Van der Meijde et al.*, 2003] and H - κ [*Zhu and Kanamori*, 2000] methods, respectively. Compared to the H - κ stacks, the contours of the waveform misfit stacks generally have a smaller trade off between H and ν and a well constrained single minimum for the preferred solution. Nonetheless, for most stations the two methods yield similar results (H is usually within the uncertainty estimates). For stations IGPB and NOVB we obtained an estimate only with the H - κ stacking method, and for AQDB only with the waveform method. For stations BEB, IGCB, SAMB and STMB data quality did not allow for reliable stacking results.

[14] A thinner crust (~30–34 km) is found beneath stations AQDB, ARAB and PP1B, which are located on the northwestern margin of the Paraná basin (Figure 1), as well as CAUB and CS6B, which are near the eastern South American margin in the Borborema province. Thicker crust (>40 km) is found beneath BALB on the S edge of the Guyana shield, IGPB and NP4B on the E edge of the Paraná basin, ITAB in the S Paraná basin and ITPB in the Mantiqueira fold belts (Brasiliano Orogen, 0.5–0.9 Ga) [*de Almeida et al.*, 2000], just as they meet the São Francisco craton, which is the oldest part of South America. The remaining stations all have intermediate crustal thicknesses.

3.2. RF Inversion

[15] The inversion results for all stations are shown in Figure 6. The synthetic RFs do not show the same troughs directly before and after the direct P arrival as is seen in the observed RFs because we do not use a high pass filter during the computation of the synthetic RFs. The troughs surrounding the peaks are a result of noise and of filtering and also seen in the results of deconvolving the vertical component with itself. The troughs largely do not represent crustal structure and we do not interpret them as such. We adjust the layers of the starting model to achieve a good alignment of peaks in the respective RFs. This also minimizes the misfit without producing artifacts in the crustal model because of the troughs in the RF. The RF stacks for stations AQDB, BALB, IGPB and NP4B did not allow resolving intracrustal features. For these stations we approximate the crust as homogeneous using the velocities from the grid search.

3.3. Continuous Moho Depths

[16] The Moho depths throughout South America are mostly within the range of 40 ± 10 km (Figure 7). The most prominent exception is the Central Andes with Moho depths up to 68 km. The deepest Moho outside of the Andes is found in the Amazon craton, where the Moho is more than 50 km deep in the eastern Guyana shield. This region of deep Moho continues through the Amazonas Basin into the Guaporé shield, to form a large NNW–SSE lying zone of deep Moho. The western parts of the Guyana and Guaporé shields, as well as to a certain degree the Amazonas basin, feature a shallower Moho. Therefore, the N–S changes in tectonic domain are in contrast to the E–W changes in Moho depth. This theme of Moho depth not corresponding with tectonic region as outlined in Figure 7 continues in most other regions; for example, the Moho of the western Paraná basin is deeper than its eastern part and the deeper Moho of the western Mantiqueira province extends into the central São Francisco craton. The
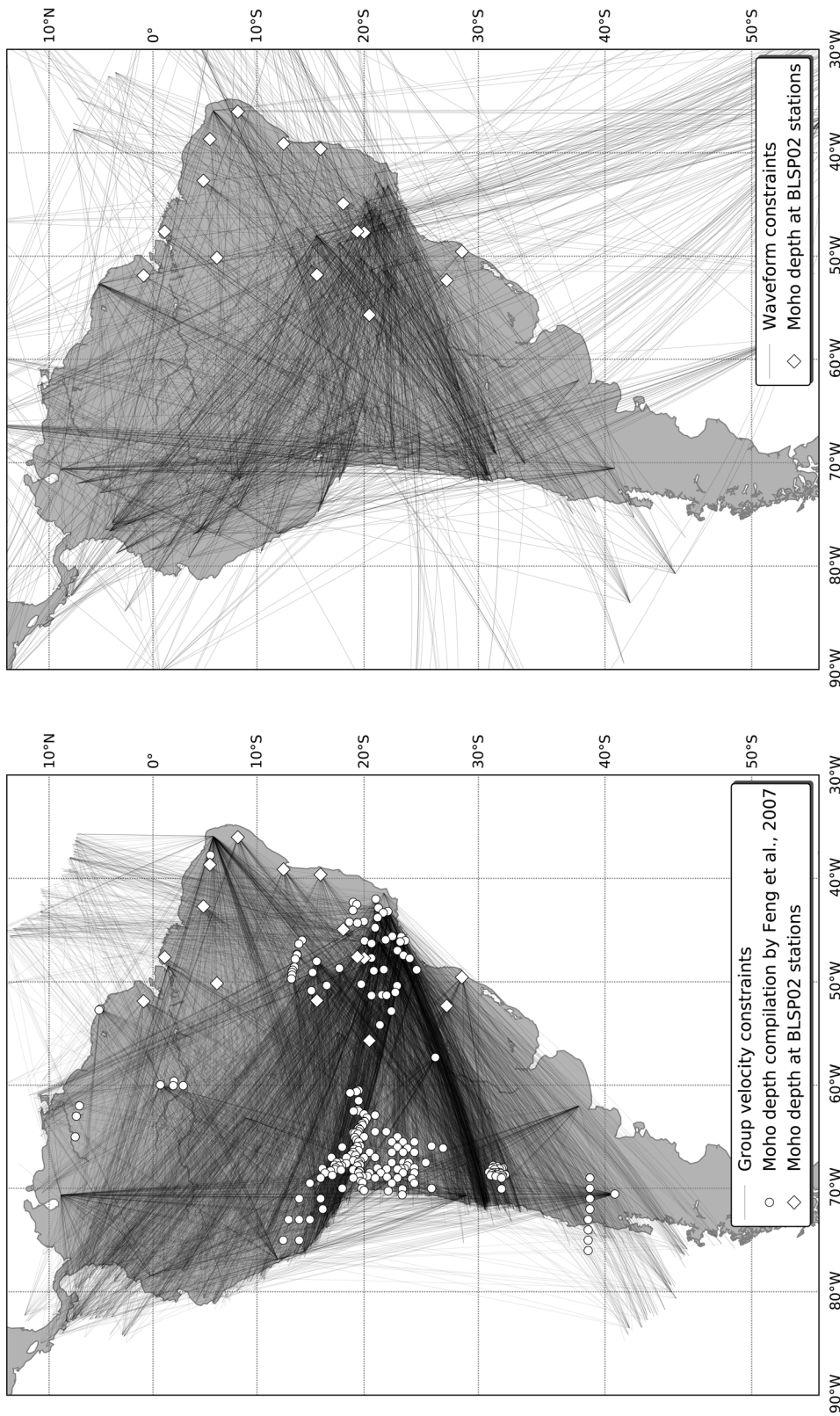
Figure 3. The wave paths of the group (left) velocity data and (right) waveform data used for the inversion. The circles and the diamonds in Figure 3 (left) correspond to the locations of the existing and new Moho depth point constraints, respectively. The diamonds in Figure 3 (right) show the locations of new BLSP02 point constraints only.

Table 1. Summary of Moho Depth and Poisson's Ratio Found for the BLSP02 Stations[a]

Station	Waveform Stacking		Traveltime Stacking		Crust2.0	
	H (km)	ν	H (km)	ν	H (km)	Age (Ma)
AQDB			31.3 ± 1.2	0.263 ± 0.013	41	1900
ARAB	31.4 ± 1.2	0.283 ± 0.073	29.6 ± 1.3	0.297 ± 0.013	41	1750
BALB	42.3 ± 1.4	0.260 ± 0.007	41.4 ± 1.3	0.269 ± 0.011	41	2750
BEB					42	2250
CAUB	34.2 ± 0.6	0.267 ± 0.052	33.8 ± 0.7	0.273 ± 0.008	37	2000
CRJB	37.1 ± 1.2	0.262 ± 0.027	36.2 ± 0.9	0.266 ± 0.009	37	2900
CS6B	31.0 ± 0.9	0.238 ± 0.053	30.3 ± 1.0	0.252 ± 0.016	39	2500
IGCB					42	2250
IGPB	44.5 ± 0.8	0.224 ± 0.042			41	2250
ITAB	42.5 ± 1.6	0.255 ± 0.029	42.3 ± 1.4	0.260 ± 0.013	41	2750
ITPB	40.3 ± 0.9	0.262 ± 0.022	39.9 ± 0.9	0.266 ± 0.010	32	2750
NOVB	38.5 ± 1.1	0.257 ± 0.050			32	1750
NP4B	40.8 ± 1.6	0.260 ± 0.068	40.5 ± 0.9	0.267 ± 0.010	40	2250
PDCB	37.3 ± 0.7	0.248 ± 0.017	36.6 ± 0.7	0.260 ± 0.008	32	2700
PP1B	33.5 ± 0.7	0.235 ± 0.051	33.3 ± 0.8	0.242 ± 0.012	41	1750
SAMB					41	1750
SNVB	34.8 ± 1.1	0.279 ± 0.031	36.0 ± 0.9	0.250 ± 0.012	31	2600
STMB					39	2750
TRMB	38.0 ± 0.8	0.239 ± 0.025	37.4 ± 0.8	0.258 ± 0.009	37	2750
TRSB	37.4 ± 0.5	0.255 ± 0.013	37.4 ± 0.6	0.251 ± 0.009	39	3250

[a]The age at the station locations are determined using digitized maps from *Cordani and Sato* [1999]. For comparison, we also show crustal thickness predicted in Crust2.0 [*Bassin et al.*, 2000].

inhomogeneous crustal thickness of the Tocantins has been previously resolved [*Assumpção et al.*, 2004] and has been interpreted as isostatic compensation of the local topography. A shallow Moho (≈30 km) is imaged in the foreland basin system east of the Central Andes in the northern Chaco Basin and westernmost Paraná basin. This shallow zone extends to the north where it is bounded by the Andes and the Guaporé Shield. This region of shallow Moho also features positive gravity anomalies [*Chapin*, 1996], indicating possible flexure of a rigid lithosphere supporting the thin crust [*Beck et al.*, 1996]. As expected from the data coverage (Figure 3) we get poor resolution at latitudes south of roughly 40°S and in oceanic areas (in particular the Pacific).

4. Discussion

4.1. Crustal Structure

[17] The results obtained using the two different stacking methods differ slightly, but generally within the uncertainty estimate. Figure 8 compares the crustal thickness and Poisson's ratio from our analysis beneath stations of different lithospheric formation age, which we take from [*Cordani and*
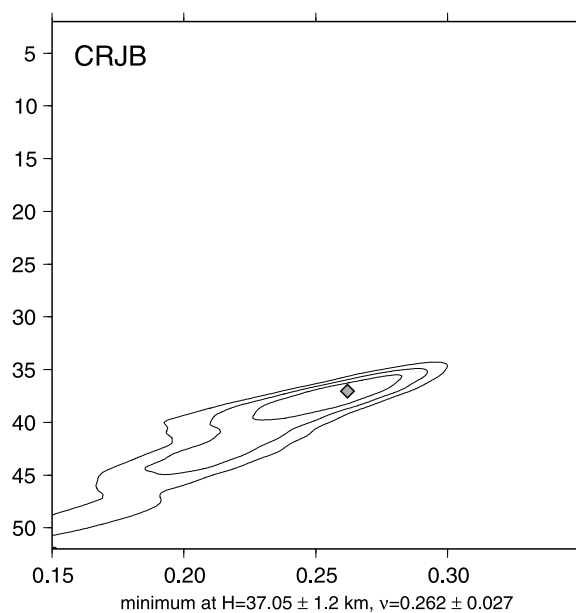

minimum at H=37.05 ± 1.2 km, ν=0.262 ± 0.027

Figure 4. Contour plot on the resulting grid from a waveform misfit stack [*Van der Meijde et al.*, 2003].
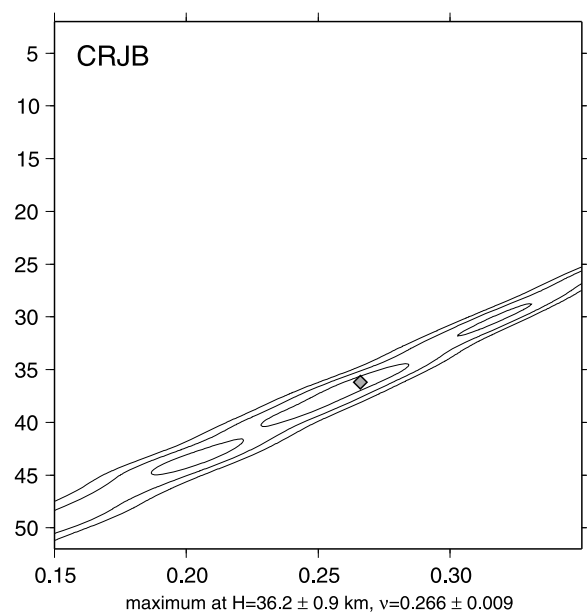

maximum at H=36.2 ± 0.9 km, ν=0.266 ± 0.009

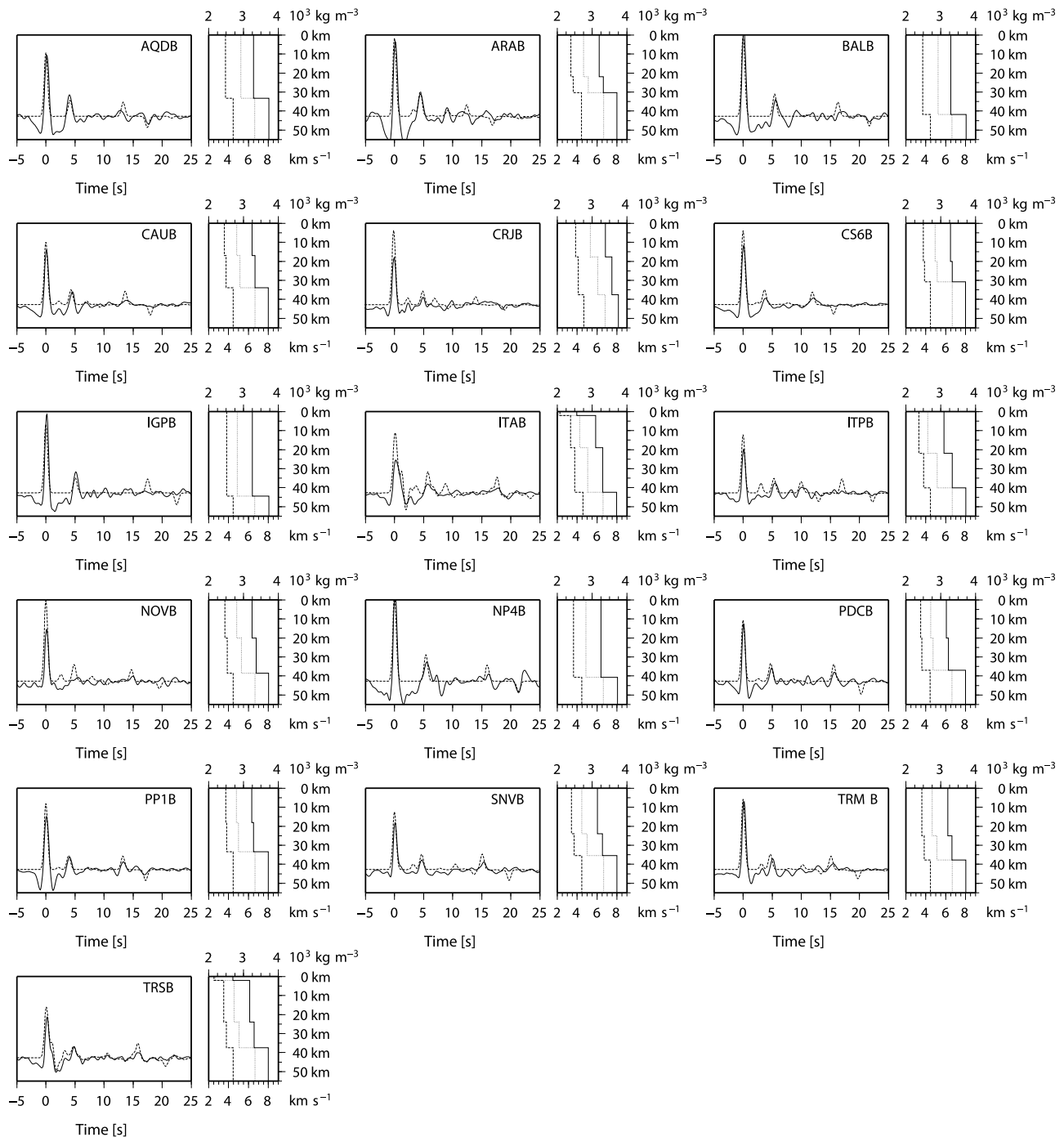**Figure 5.** Same as Figure 4 but for the method of *Zhu and Kanamori* [2000].

Figure 6. Synthetic (dashed lines) and observed (solid lines) RFs. The smaller boxes show *P* velocity (solid lines), *S* velocity (dashed), and density (dotted) for the best fitting simple model.

Sato, 1999]. The maps of lithospheric age they provide have 500 Ma contour level increments, so we average our results over bins of the same 500 Ma width. Using first only the BLSP02 results we obtained from the two stacking methods we identify a slight but insignificant trend for Crustal thickness *H* but not for Poisson's ratio ν (Figure 8a). *H* increases with increasing geologic age. When using both the BLSP02 and prior results we find a trend for the Poisson's ratio ν, which is now lower for older crust, perhaps indicating a more felsic composition of the older crust [*Christensen*, 1996]. However, the *H* constraints no longer yield a trend when using all stations. In particular, there is no indication of a thinner Archean compared to Proterozoic crust as seen in other parts of the world [*Durrheim and Mooney*, 1991, 1994; *Ramesh et al.*, 2002; *Clitheroe et al.*, 2000; *Dahl-Jenson et al.*, 2003]. Precambrian South America corresponds better to Moho results found for example in Southern India [*Gupta et al.*, 2003] or the Arabian plate [*Al-Damegh et al.*,
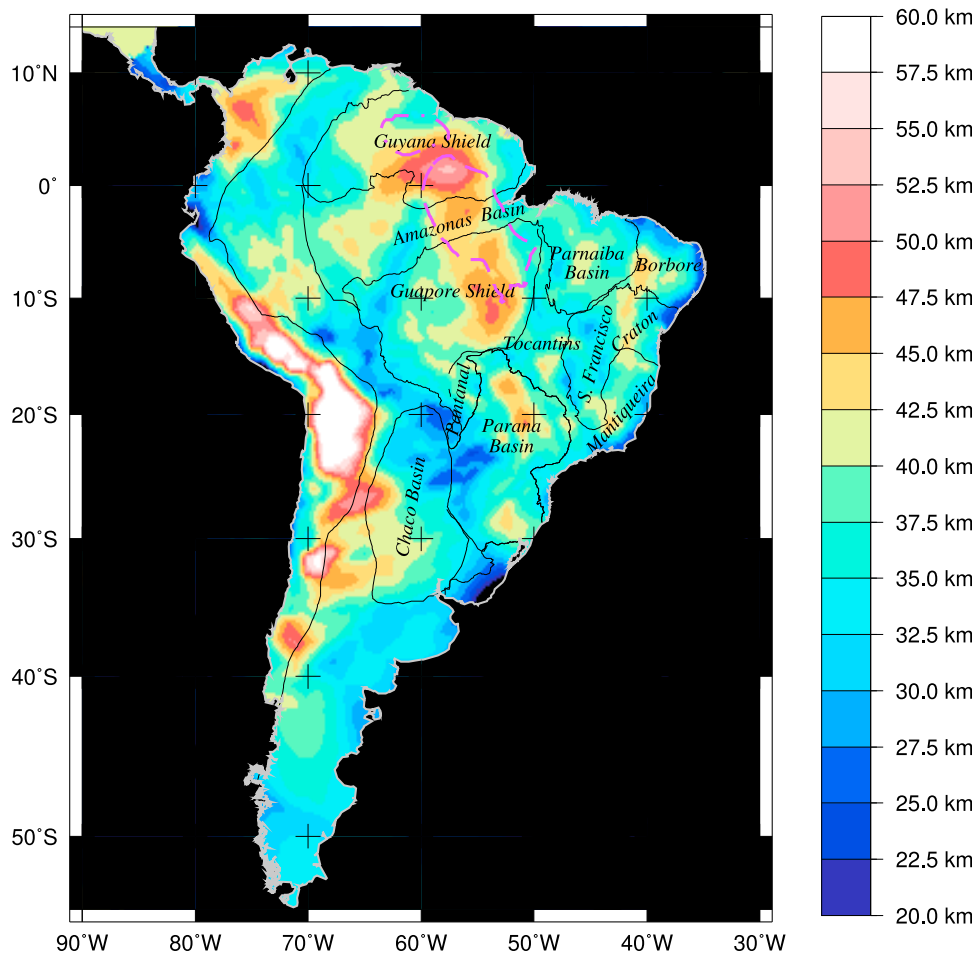
Figure 7. Map of the Moho depth obtained from the joint inversion. The purple lines mark the areas of the Central Amazonian province (>2.3 Ga) from *Tassinari and Macambira* [1999].

2005], where there also does not appear to be a significant difference in the crustal thickness between Archean and Proterozoic provinces.

[18] For the RF inversion we group the stations according to their geologic or geographic domains:

[19] 1. Stations AQDB, PP1B, ARAB, IGPB, and NP4B all lie around the rim of the Paraná basin. AQDB, PPQB, and ARAB lie to the NW and feature a crustal thickness of about 33 km and some intracrustal structure. IGPB and NP4B are to the NE and feature a thicker crust of about 40 km, with no resolvable interface between the Moho and the surface.

[20] 2. Stations CRJB, ITPB, PDCB, SNVB, and TRMB are located within or on the edge of shields. The RF inversion for these stations yields a midcrustal interface at intermediate depth.

[21] 3. Stations ITAB and TRSB are located in platforms. These stations indeed require a sediment cover to fit the RFs.

[22] 4. Stations CAUB, CS6B, and NOVB are in fold belts. We model a midcrustal interface similar to the stations located in shields (group 2).

[23] 5. Station BALB presents a special case. The station lies on the edge of the Guyana shield and Amazon basin. The RF suggests some intracrustal structure but, as some stations from group 1, can also be modeled with a homogeneous crust.

4.2. Moho Map

[24] Our new Moho map (Figure 7) better resolves the Moho in eastern South America than previous models, as we use new RF constraints in that region for the inversion. The effect they have on the inversion is visible in Figure 9, where we compare the Moho depth obtained from the inversion at the station locations with and without the new point constraints. We see differences greater than 7 km and a mean difference of 3.6 km. The desired result from the joint inversion is that the final model adheres relatively closely to the point constraints. Because the RF point constraints are also input data for the inversion we expect to retrieve them in the final model. However, since similar Moho depths at those locations cannot be retrieved in the model without new constraints these differences illustrates the critical importance of the new point constraints. In a resolution test an input model using 700 km blocks with Moho variations of 40 ± 10 km is mostly well recovered, with smearing occurring in the southern tip of South America and in the Pacific and Atlantic oceans (Figure 10). This behavior was expected considering the data coverage (Figure 3).

[25] With the continuous sampling of the Moho provided by our map we again search for trends with geologic age
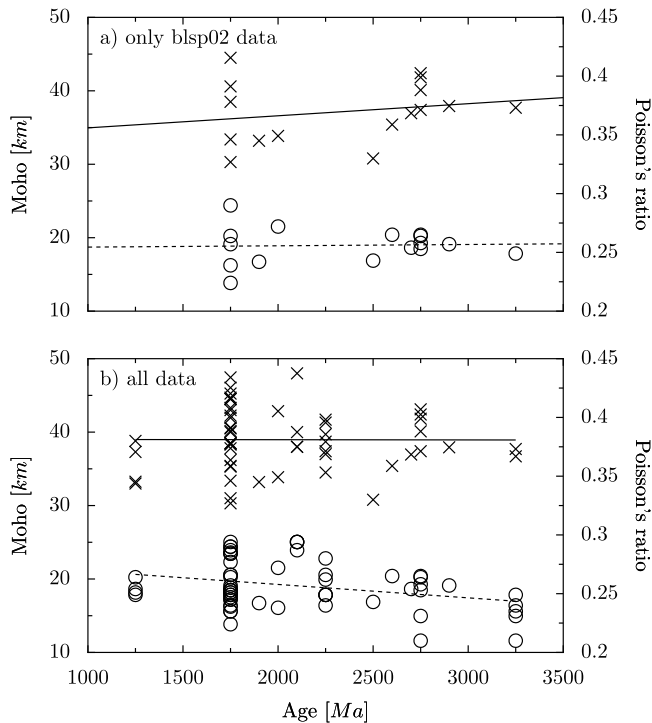
Figure 8. (a) Moho depth (crosses) and Poisson's ratio (circles) obtained from RF analysis of the BLSP02 stations versus lithospheric age. (b) Same as Figure 8a after combining our results with additional data from the literature.

(Figure 11). The map shows a change in average crustal thickness with age. There is enough variation in crustal thickness within the respective age intervals to allow satisfactory fitting of a straight line. However, since Moho depth peaks between 2.0 and 3.0 Ga and decreases toward younger and older crust a single trend might not be the best way to describe the behavior of Moho thickness with lithospheric age. Our observations are better described by fitting two lines to our data using Moho depths before and after 2.5 Ga, respectively (Figure 11). The trend with age of the continuous Precambrian Moho is different compared to the one from the RFs alone (Figure 8b). This suggests a possible sampling bias for conclusions obtained from receiver functions alone because incomplete sampling can produce apparent trends or correlations.

[26] By continuously sampling the Moho, Moho topography (spatial variations of the lateral changes in thickness) and its relation to geologic age can also be investigated. Figure 12 shows the gradient in Moho depth from our Moho map versus geologic age of Precambrian South America. Buoyancy forces and lower crustal flow may smooth out Moho topography over time [*McKenzie et al.*, 2000]. The Moho topography has an inverse behavior with respect to age from that of the Moho thickness; the thicker crust of 2.0–2.5 Ga and 2.5–3.0 Ga is smoother than Precambrian crust of both younger and older age. The steepness of the slopes we obtain depends somewhat on how strongly we damp or flatten our model during the inversion. However, regardless of how strongly we damp or smooth our model, we always obtain the same Moho topography pattern. The same behavior of the Moho is observed after inversion without point constraints, showing that it is not

caused by the irregular spacing of the RF point constraints and their dominant local influence in the joint inversion.

[27] A prominent new feature compared to previous Moho models [*Feng et al.*, 2007] is the thick crust in parts of the Amazonian Craton. The Amazonian Craton consists of three main geological provinces: the Precambrian Guyana and Guaporè Shields and the Mesozoic Amazon basin lying in between the shields (Figure 7). The Guyana shield has an average elevation of 1200 m and reaches up to 3000 m in the Guyana highlands; however, we note that (1) the highest elevations occur to the NW of the thickest crust and (2) isostatic correction of topography (using densities from *Chapin* [1996]) does not remove the strong anomalies. Hence, the crustal thickening cannot be explained simply by isostatic compensation of the relief. *Tassinari and Macambira* [1999] identify six geochronological provinces. The oldest units are the Archean Nuclei (Xingu and Pakaraima) that comprise the Central Amazonian and are surrounded by mostly Paleoproterozoic provinces. The geochronological provinces are oriented perpendicular to the geological provinces. The NNW–SSE region of increased crustal thickness corresponds roughly to the Central Amazonian province (dashed line in Figure 7); thus, the thicker crust in that part of the Amazonian is likely related to its lithospheric age. *Feng et al.* [2007] find higher velocities in the underlying mantle, and conclude that the Amazonian craton was not deeply affected by the rifting events during the basin evolution [*de Almeida et al.*, 2000]. *Schmitz et al.* [2002] conducted a seismic refraction experiment in the northernmost part of the zone with increased crustal thickness, and also find large thicknesses of up to 50 km. They attribute this greater thickness to a possible plume during the Paleozoic.

5. Conclusions

[28] We analyzed receiver functions from 20 temporary seismic stations deployed in eastern South America, to provide constraints on crustal thickness and average Poisson's
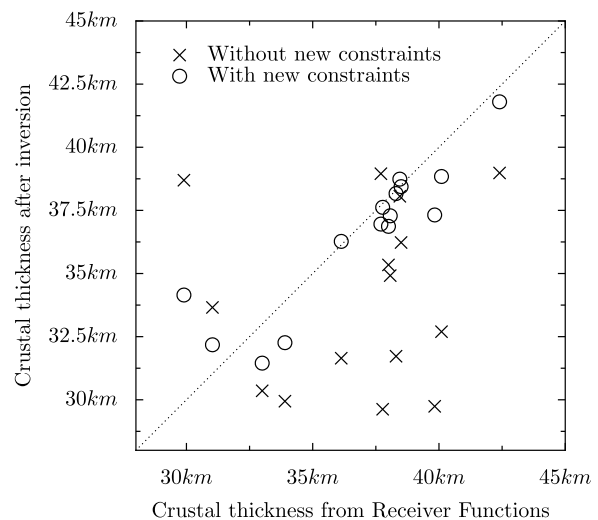

Figure 9. Comparison of the Moho depths at the BLSP02 station locations obtained from receiver functions and joint inversion with (circles) and without (crosses) using new point constraints.
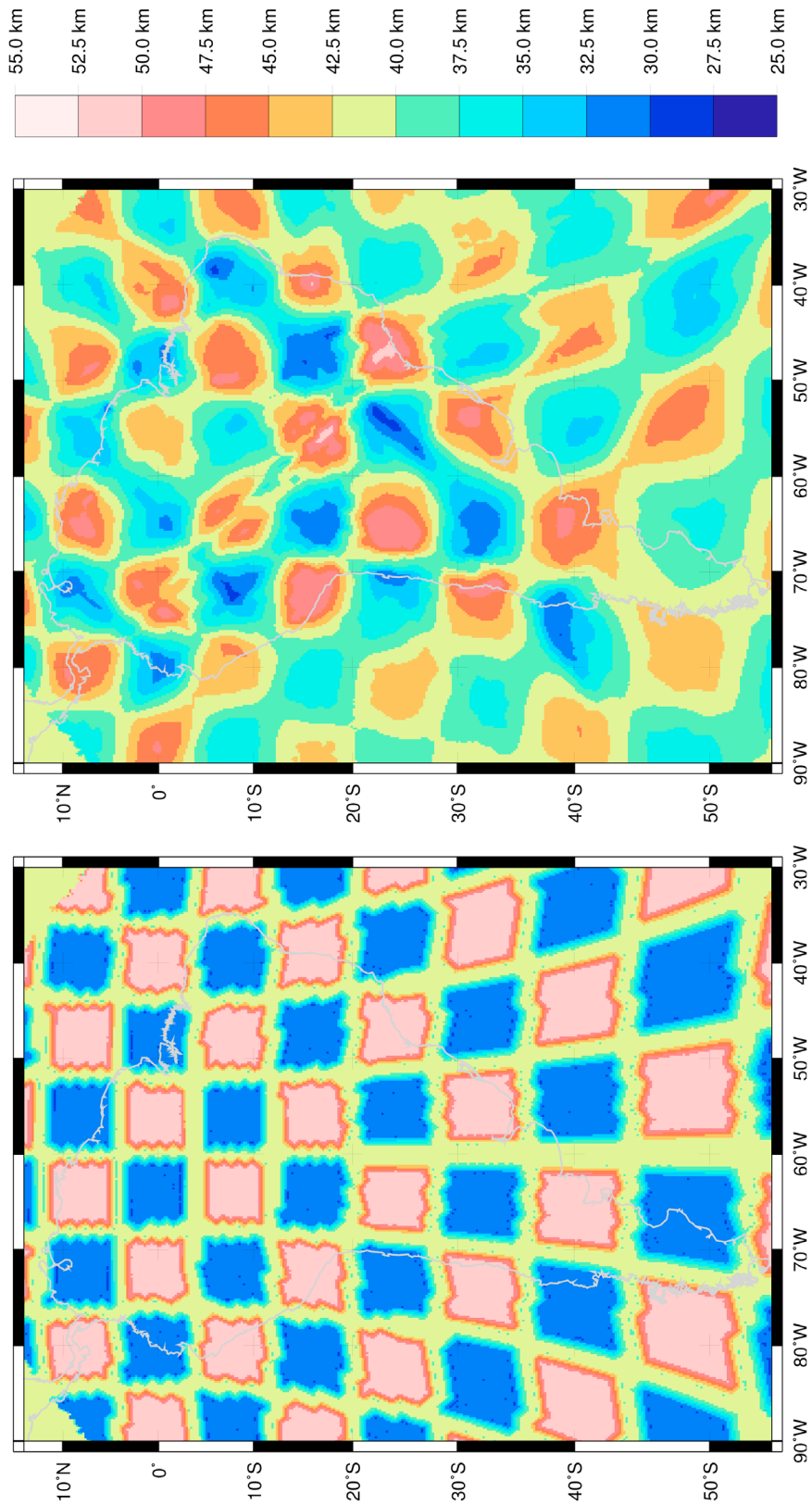
Figure 10. (right) Resolution test using synthetic data generated from the checkerboard model. (left) Inversion of these data indicates generally good resolution for most of continental South America.

ratio for locations in previously undersampled areas of South America. Crustal thickness and Poisson's ratio are obtained using two stacking methods [*Zhu and Kanamori*, 2000; *Van der Meijde et al.*, 2003], which provide similar results for Moho depth for 13 of the 20 stations. For four stations no Moho could be identified and for three only one of the methods identifies the Moho. Our new constraints combined with results from previous RF studies yield a total of 67 point constraints on the Precambrian crust of eastern South America. In older crust we find slightly lower Poisson's ratios, which could suggest a more felsic composition compared to the younger provinces. The average thickness of Archean crust appears to be similar to that of Proterozoic crust.

[29] We have derived a new, continuous Moho map by interpolating the RF constraints through a joint inversion of such Moho point constraints with Rayleigh wave group velocities and waveforms. Unlike the individual receiver functions, our new map shows a slight change in crustal thickness with age. Moho depth is largest for crustal ages between 2.0 and 3.0 Ga, and decreases toward younger and older crust. This is noteworthy, as the analysis with the Moho map samples the crust regularly. This eliminates the possibility of a sampling bias and provides a benchmark for the results from RF analysis; since we obtain a different age dependence of the Moho depth from the RFs and the Moho map we conclude the one derived from the RFs is possibly biased.

[30] The continuous sampling in our map also provides Moho topography, which likewise shows an age dependence. The Moho is flattest between 2.0 and 3.0 Ga, and rougher for younger and older crust.

[31] The limited quality of the RFs precludes a detailed investigation of intracrustal structure. We obtained first-order constraints on intracrustal structure by using 1–3 layers in a RF inversion exercise. Overall we find that for most stations we can model the RFs with a relatively uniform crust. Two stations require sediment covers for a satisfactory fit of the RFs. In the shield and fold belt regions we retrieve intracrustal structures at intermediate depths between 15 and 20 km.

[32] Our new, continuous Moho map is consistent with previously published maps [*Feng et al.*, 2007] as well as with Crust2.0 [*Bassin et al.*, 2000], where Crust2.0 is constrained
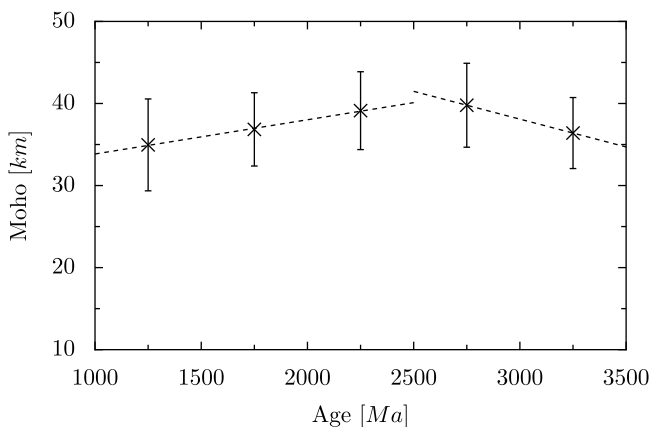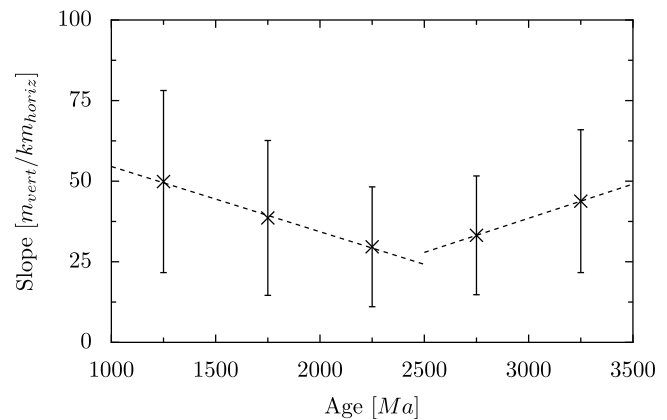

Figure 12. Same as Figure 11 but for the Moho topography.

by data. Moho depth and Moho flatness peak between 2.0 and 3.0Ga and decrease for older and younger crust. Our map shows a large region with an up to 50km thick crust in the Amazon craton that roughly coincides with the Central Amazonian Province, which is the oldest lithospheric core of the Amazon craton [*Tassinari and Macambira*, 1999].

References

Al-Damegh, K., E. Sandvol, and M. Barazangi (2005), Crustal structure of the Arabian plate: New constraints from the analysis of teleseismic receiver functions, *Earth Planet. Sci. Lett.*, *231*, 177–196, doi:10.1016/j.epsl.2004.12.020.

Ammon, C. (1991), The isolation of receiver effects from teleseismic *P* waveforms, *Bull. Seismol. Soc. Am.*, *81*, 2504–2510.

Ammon, C., G. Randall, and G. Zandt (1990), On the nonuniqueness of receiver function inversions, *J. Geophys. Res.*, *95*(B10), 15,303–15,318, doi:10.1029/JB095iB10p15303.

An, M., and M. Assumpção (2006), Crustal and upper mantle structure in the intracratonic Paraná Basin, SE Brazil, from surface wave dispersion using genetic algorithms, *J. South Am. Earth Sci.*, *21*(3), 173–184, doi:10.1016/j.jsames.2006.03.001.

Assumpção, M., D. James, and A. Snoke (2002), Crustal thickness in SE Brazilian shield by receiver function analysis: Implications for isostatic compensation, *J. Geophys. Res.*, *107*(B1), 2006, doi:10.1029/2001JB000422.

Assumpção, M., M. Bianchi, and M. Schimmel (2003), Francisco Craton, SE Brazilian Shield, by slant stacking of receiver functions, *Eos Trans. AGU*, Fall Meet. Suppl., Abstract S41D-0108.

Assumpção, M., A. Meijian, M. Bianchi, G. França, M. Rocha, J. Barbosa, and J. Berrocal (2004), Seismic studies of the Brasília fold belt at the western border of the São Francisco Craton, central Brazil, using receiver function, surface-wave dispersion and teleseismic tomography, *Tectonophysics*, *388*, 173–185, doi:10.1016/j.tecto.2004.04.029.

Bassin, C., G. Laske, and G. Masters (2000), The current limits of resolution for surface wave tomography in North America, *Eos Trans. AGU*, *81*(48), Fall Meet. Suppl., Abstract S12A-03.

Beck, S., G. Zandt, S. Myers, T. Wallace, P. Silver, and L. Drake (1996), Crustal-thickness variations in the central Andes, *Geology*, *24*(5), 407–410, doi:10.1130/0091-7613(1996)024<0407:CTVITC>2.3.CO;2.

Beurlen, K. (1970), *Geologie von Brasilien*, Gebrüder Borntraeger, Berlin.

Chang, S., et al. (2010), Joint inversion for 3-dimensional *S* velocity mantle structure along the Tethyan margin, *J. Geophys. Res.*, *115*, B08309, doi:10.1029/2009JB007204.

Chapin, D. (1996), A deterministic approach toward isostatic gravity residuals—A case study from South America, *Geophysics*, *61*(4), 1022–1033, doi:10.1190/1.1444024.

Figure 11. Mean Moho depth from the joint inversion versus lithospheric age for the entire Precambrian crust.

Christensen, N. (1996), Poisson's ratio and crustal seismology, *J. Geophys. Res.*, *101*(B2), 3139–3156, doi:10.1029/95JB03446.

Christensen, N., and W. Mooney (1995), Seismic velocity structure and composition of the continental crust: A global view, *J. Geophys. Res.*, *100*(B6), 9761–9788, doi:10.1029/95JB00259.

Clitheroe, G., O. Gudmundsson, and B. Kennett (2000), The crustal thickness of Australia, *J. Geophys. Res.*, *105*(B6), 13,697–13,713, doi:10.1029/1999JB900317.

Coffin, M., and O. Eldholm (1994), Large igneous provinces: Crustal structure, dimensions, and external consequences, *Rev. Geophys.*, *32*(1), 1–36, doi:10.1029/93RG02508.

Cordani, U., and K. Sato (1999), Crustal evolution of the South American platform, based on Nd isotopic systematics on granitoid rocks, *Episodes*, *22*(3), 167–173.

Dahl-Jensen, T., et al. (2003), Depth to Moho in Greenland: Receiver-function analysis suggests two Proterozoic blocks in Greenland, *Earth Planet. Sci. Lett.*, *205*(3–4), 379–393, doi:10.1016/S0012-821X(02)01080-4.

de Almeida, F., B. B. Benjamim, and C. Carneiro (2000), Origin and evolution of the South American platform, *Earth Sci. Rev.*, *50*, 77–111, doi:10.1016/S0012-8252(99)00072-0.

Durrheim, R., and D. Mooney (1991), Archean and Proterozoic crustal evolution: Evidence from crustal seismology, *Geology*, *19*, 606–609, doi:10.1130/0091-7613(1991)019<0606:AAPCEE>2.3.CO;2.

Durrheim, R., and W. Mooney (1994), Evolution of the Precambrian lithosphere: Seismological and geochemical constraints, *J. Geophys. Res.*, *99*(B8), 15,359–15,374, doi:10.1029/94JB00138.

Feng, M., M. Assumpção, and S. van der Lee (2004), Group-velocity tomography and lithospheric S velocity structure of the South American continent, *Phys. Earth Planet. Inter.*, *147*, 315–331, doi:10.1016/j.pepi.2004.07.008.

Feng, M., S. van der Lee, and M. Assumpção (2007), Upper mantle structure of South America from joint inversion of waveforms and fundamental mode group velocities of Rayleigh waves, *J. Geophys. Res.*, *112*, B04312, doi:10.1029/2006JB004449.

França, G., and M. Assumpção (2004), Crustal structure of the Ribeira fold belt, SE Brazil, derived from receiver functions, *J. South Am. Earth Sci.*, *16*(8), 743–758, doi:10.1016/j.jsames.2003.12.002.

Gupta, S., S. Rai, K. Prakasam, D. Srinagesh, B. Bansal, R. Chadha, K. Priestly, and V. Gaur (2003), The nature of the crust in southern India: Implications for Precambrian crustal evolution, *Geophys. Res. Lett.*, *30*(8), 1419, doi:10.1029/2002GL016770.

Jacques, J. M. (2003), A Tectonostratigraphic synthesis of the sub-Andean basins: Inferences on the position of South American intraplate accommodation zones and their control on South Atlantic opening, *J. Geol. Soc.*, *160*(5), 703–717, doi:10.1144/0016-764902-089.

Kennett, B. L. N. (1983), *Seismic Wave Propagation in Stratified Media*, 342 pp., Cambridge Univ. Press, Cambridge, U. K.

Kind, R., G. L. Kosarev, and N. V. Petersen (1995), Receiver functions at the stations of the German Regional Seismic Network (GRSN), *Geophys. J. Int.*, *121*, 191–202, doi:10.1111/j.1365-246X.1995.tb03520.x.

Krüger, F., F. Scherbaum, J. Rosa, R. Kind, F. Zetsche, and J. Höhne (2002), Crustal and upper mantle structure in the Amazon region (Brazil) determined with broadband mobile stations, *J. Geophys. Res.*, *107*(B10), 2265, doi:10.1029/2001JB000598.

Langston, C. (1979), Structure under Mount Rainier, Washington, inferred from teleseismic body waves, *J. Geophys. Res.*, *84*(B9), 4749–4762, doi:10.1029/JB084iB09p04749.

McKenzie, D., F. Nimmo, and J. Jackson (2000), Characteristics and consequences of flow in the lower crust, *J. Geophys. Res.*, *105*(B5), 11,029–11,046, doi:10.1029/1999JB900446.

Owens, T., G. Zandt, and S. Taylor (1984), Seismic evidence for an ancient rift beneath the Cumberland Plateau, Tennessee: A detailed analysis of broadband teleseismic P waveforms, *Bull. Seismol. Soc. Am.*, *77*, 7783–7795.

Paige, C. C., and M. A. Saunders (1982), LSQR: An algorithm for sparse linear equations and sparse least squares suan, *Trans. Math. Software*, *8*(1), 43–71, doi:10.1145/355984.355989.

Ramesh, D., R. Kind, and X. Yuan (2002), Receiver function analysis of the North American crust and upper mantle, *Geophys. J. Int.*, *150*(1), 91–108, doi:10.1046/j.1365-246X.2002.01697.x.

Riccomini, C., and M. Assumpção (1999), Quaternary tectonics in Brazil, *Episodes*, *22*(3), 221–225.

Schmitz, M., D. Chalbaud, J. Castillo, and C. Izarra (2002), The crustal structure of the Guayana Shield, Venezuela, from seismic refraction and gravity data, *Tectonophysics*, *345*(1–4), 103–118, doi:10.1016/S0040-1951(01)00208-6.

Tassinari, C., and M. Macambira (1999), Geochronological provinces of the Amazonian craton, *Episodes*, *22*(3), 174–182.

Turner, S., M. Regelous, S. Kellet, D. Hawkesworth, and M. Mantovani (1994), Magmatism and continental breakup in the South Atlantic, *Earth Planet. Sci. Lett.*, *121*, 333–348, doi:10.1016/0012-821X(94)90076-0.

van der Lee, S., and G. Nolet (1997), Upper mantle S velocity structure of North America, *J. Geophys. Res.*, *102*(B10), 22,815–22,838, doi:10.1029/97JB01168.

van der Lee, S., D. James, and P. Silver (2001), Upper mantle S velocity structure of central and western South America, *J. Geophys. Res.*, *106*(B12), 30,821–30,834, doi:10.1029/2001JB000338.

Van der Meijde, M., S. van der Lee, and D. Giardini (2003), Crustal structure beneath broadband seismic stations in the Mediterranean Region, *Geophys. J. Int.*, *152*(3), 729–739, doi:10.1046/j.1365-246X.2003.01871.x.

Yuan, X., S. Sobolev, and R. Kind (2002), Moho topography in the central Andes and its geodynamic implications, *Earth Planet. Sci. Lett.*, *199*(3–4), 389–402, doi:10.1016/S0012-821X(02)00589-7.

Zandt, G., and C. Ammon (1995), Continental crust composition constrained by measurements of crustal Poisson's ratio, *Nature*, *374*, 152–154, doi:10.1038/374152a0.

Zhu, L., and H. Kanamori (2000), Moho depth variation in Southern California from teleseismic receiver functions, *J. Geophys. Res.*, *105*(B2), 2969–2980, doi:10.1029/1999JB900322.

M. Assumpção, Institute of Astronomy and Geophysics, University of São Paulo, Rua do Matao 1226, São Paulo, Brazil.

M. Feng, Institute of Geomechanics, Chinese Academy of Geological Sciences, MinZuDaXueNanLu 11, 100081, Beijing, China.

G. S. França, Observatório Sismológico-I1G/UnB, Campus Universitário Darci Ribeiro, SG 13, Asa Norte, Brasilia, Brazil.

S. M. Lloyd and S. van der Lee, Department of Earth and Planetary Sciences, Northwestern University, 1850 Campus Dr., Evanston, IL 60208-2150, USA. (simon@earth.northwestern.edu)